Indian Journal of Pure & Applied Physics
Vol. 56, February 2018, pp. 142-148

Electrical characterization of MIS diode prepared by magnetron sputtering

H Tanrıkulu, A Tataroğlu*, E E Tanrıkulu & A Büyükbaş Uluşan
Department of Physics, Faculty of Science, Gazi University, Ankara, Turkey

Received 30 May 2017; accepted 3 November 2017

TiO_2 thin film has been prepared on *n*-type Si wafer to fabricate an Au/TiO_2/n-Si (MIS) diode by RF magnetron sputtering technique. The current-voltage (*I-V*) and capacitance-voltage (*C-V*) measurements of the diode have been performed over a wide range of temperatures (240-400 K) and frequencies (10 kHz-1 MHz), respectively. From *I-V* measurements, an abnormal increase in the barrier height (Φ_b) and a decrease in the ideality factor (*n*) with increasing temperature have been observed. This temperature dependence has been attributed to the barrier in homogeneities by assuming a Gaussian distribution (GD) of barrier heights at metal/semiconductor (*M*/*S*) *interface*. Both the conventional and modified Richardson plot show linearity. The activation energy (E_a), Richardson constant (A^*) and Φ_b value have been calculated from the slope and intercept of the linear region. The obtained Richardson constant value of 113.82 A. cm^{-2}. K^{-2} is in close agreement with the known value of 112 A.cm^{-2}. K^{-2} for *n*-Si. The interface state density (N_{ss}) and series resistance (R_s) of the diode has been obtained from the *I-V* measurements. In addition, the Φ_b value was determined from C^{-2}-*V* characteristics. The obtained results indicate that the MIS diode with TiO_2 interfacial insulator layer can be used in many device applications.

Keywords: MIS diode, TiO_2 thin film, Ideality factor, Barrier height, Interface states, Series resistance

1 Introduction

The direct contact between a metal and a semiconductor forms a metal-semiconductor (MS) Schottky diode. However, the interfacial insulator layer such as TiO_2, SnO_2 and SiO_2 between metal and semiconductor converts the MS diode into metal-insulator-semiconductor (MIS)-type Schottky diode. The MIS Schottky diodes due to the presence of the insulator layer have advantages such as lower leakage current and higher rectification ratio. Also, the performance of Schottky diodes depends on several parameters such as temperature, homogeneity of the insulator layer, interface states (N_{ss}), and series resistance (R_s). These parameters have a strong influence on the electrical characteristics of Schottky diodes[1-3].

The current-voltage (*I-V*) characteristics measured only at room temperature do not give detailed information about the current conduction mechanism. Therefore, to better understand current-transport mechanism and barrier formation between metal and semiconductor, the *I-V* characteristics of Schottky diodes should be measured over a wide temperature range. To analyze the *I-V* characteristics of MS and MIS diodes, the most common approach is pure thermionic emission of carriers over the barrier. Generally, the thermionic emission (TE) mechanism is used to extract the main diode parameters. Analysis of the *I-V* characteristics based on TE theory usually reveals an abnormal decrease in the barrier height and an increase in the ideality factor with decreasing temperature. The abnormal behavior is attributed to Schottky barrier inhomogeneities[4-10].

Titanium dioxide (TiO_2) has significant properties such as high chemical stability, high photocatalytic activity, low toxicity, high refractive index and easy availability. TiO_2 has been used in many applications such as gas sensors, photocatalysts, thin film capacitor, dye-sensitized solar cells and photovoltaic devices. To prepare TiO_2 thin film various methods have been developed such as sol-gel, pulsed laser deposition, drop-casting, electrochemical etching, metal organic chemical vapor deposition and magnetron sputtering[11-15]. TiO_2 contains three main crystalline phases such as anatase, rutile and brookite. The anatase and rutile phases are tetragonal structure, and they can synthesize in the thin film form. The anatase structure is obtained at low temperatures of around 350 °C. The TiO_2 in the form of anatase phase is the most preferred for photoelectrochemical applications. The rutile phase is also present at temperatures between 400 and 800 °C. At higher temperatures, only the rutile structure is present[16-20].'

The purpose of this study is to investigate the effect of temperature on electrical characteristics of the prepared Au/TiO_2/n-Si (MIS) diode. The MIS diode

*Corresponding author (E-mail: ademta71@gmail.com)

parameters have been extracted from the current-voltage (*I-V*) and capacitance-voltage (*C-V*) characteristics.

2 Experimental Details

The Au/TiO_2/*n*-Si (MIS) structure was fabricated on phosphorus doped (*n*-type) single crystal Si substrate with a 2" diameter, 280 µm thickness, (111) orientation, and 4.45 Ω.cm, resistivity. Before the fabrication process, the substrate was chemically cleaned using the conventional method and then chemically etched and finally quenched in de-ionized water (resistivity of 18 MΩ.cm). After the cleaning and etching process, the substrate was mounted on a stainless steel sputtering holder that was heated optically and loaded into a radio frequency (RF) magnetron sputtering system. When the vacuum has reached 10^{-8} mbar, the Si substrate was heated up to 200 °C and sputter cleaned in pure argon ambient to ensure the removal of any residual organics. After the substrate preparation, the Si substrate was transferred into the deposition chamber to deposit TiO_2 film from high purity (99.999%) Ti target, under specific Ar+O_2 reactive gas mixture (Ar/O_2=90/10 sccm) controlled by mass flow controllers. During the TiO_2 film deposition, the substrate temperature and the pressure were set to 200 °C and 3×10^{-2} mbar, respectively.

For the electrical characterization, firstly the ohmic back contacts were formed by deposition of high purity Au (99.999%) with a thickness of ~2000 Å at 400 °C, under 10^{-7} mbar vacuum. Then, sample was annealed at 375 °C for 7 min to achieve good ohmic contact behavior. Finally, dot shaped rectifier front contacts with 2 mm diameter and ~2000 Å thickness were formed by deposition of high purity Au (99.999%) at 50 °C. The interfacial insulator layer thickness was estimated to be about 45 Å from the insulator capacitance in the strong accumulation.

The *I-V* measurements of Au/TiO_2/n-Si (MIS) diode were performed by the use of a Keithley 2400 source-meter in the temperature range of 240-400 K using a temperature-controlled Janes vpf-475 cryostat. The diode temperature was controlled using of a Lakeshore-321 auto-tuning temperature controller with sensitivity better than ±0.1 K. The capacitance-voltage (*C-V*) measurements were carried out by using an HP 4192A LF impedance analyzer in the frequency range of 10 kHz-1 MHz and at room temperature.

3 Results and Discussion

3.1 Current-voltage characteristics

The current-voltage (*I-V*) characteristics are analyzed on the basis of conventional thermionic emission (TE) theory. According to TE theory, the current through a Schottky barrier diode with series resistance at forward bias *V*, for $V > 3kT/q$, is given by the following relation[1-3]:

$$I = I_o\left[\exp\left(\frac{q(V-IR_s)}{nkT}\right)-1\right] \quad \ldots (1)$$

where *V* is the applied bias voltage, R_s is the series resistance, *n* is the ideality factor, *k* is the Boltzmann constant and *T* is the temperature. I_0 is the reverse saturation current derived from the straight line intercept of ln (*I*) at *V*=0 and is given by:

$$I_o = A\,A^*\,T^2\,\exp\left(-\frac{q\Phi_b}{kT}\right) \quad \ldots (2)$$

where *A* is the diode area (3.14×10^{-2} cm^2), A^* is the effective Richardson constant (equal to 112 A/cm^2K^2 for *n*-Si) and Φ_b is the zero-bias barrier height. TE theory is used to determine the barrier height. The Φ_b value is obtained from Eq. (2). The *n* value can be extracted from the slope of the linear region of ln (*I*) versus *V* plot and is given by:

$$n = \frac{q}{kT}\left(\frac{dV}{d(\ln I)}\right) \quad \ldots (3)$$

Figure 1 shows the semi-logarithmic forward and reverse bias *I-V* plots of the Au/TiO_2/n-Si (MIS) diode

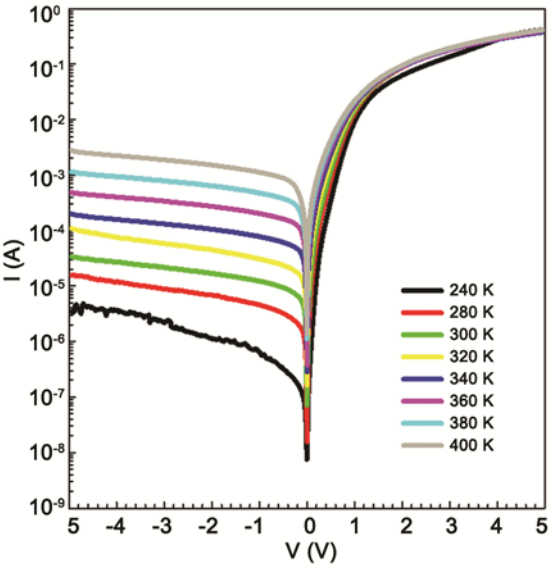

Fig. 1 — The semi-logarithmic forward and reverse *I-V* plots of the MIS diode in the temperature range of 240-400 K.

in the temperature range of 240-400 K. As seen in Fig. 1, the MIS diode exhibits a good rectifying behaviour. The reverse current increases with increasing temperature as predicted by the TE theory. But, the forward current does not change significantly with temperature. The increase can be attributed to the drift velocity of heat-generated electrons and holes in TiO_2. Furthermore, the *I-V* curves show a deviation from linearity due to the series resistance and interface states[21-26].

The values of ideality factor (n) and reverse saturation current (I_0) obtained from the slope and intercept of the forward-bias ln (I)-V curves, and barrier height (Φ_b) values calculated from the I_0 values are given in Table 1. As seen in Table 1, the ideality factor decreases while the barrier height increases with increasing temperature. Indeed, the barrier height should decrease as the temperature increases for homogeneous Schottky barrier. This abnormal behaviour can be explained by assuming a Gaussian distribution of Schottky barrier heights due to barrier inhomogeneities[7,10,21-26]. Also, the obtained values of the ideality factor are greater than ideal value of 1. The high value of n is attributed to the presence of a wide distribution of low-Schottky barrier height patches or barrier inhomogeneous.

Additionally, the barrier height and series resistance of the MIS diode can be extracted by using a method developed by Norde[27]. According to this method, Norde's function, $F(V)$, is plotted against voltage (V) and is expressed as[27,28]:

$$F(V)=\frac{V}{\gamma}-\frac{kT}{q}\ln\left(\frac{I}{AA^{*}T^{2}}\right) \quad \ldots (4)$$

where γ is an integer greater than ideality factor. The barrier height is given by:

$$\Phi_{b}=F(V_{min})+\frac{V_{min}}{\gamma}-\frac{kT}{q} \quad \ldots (5)$$

where $F(V_{min})$ is the minimum value of $F(V)$ and V_{min} is the corresponding voltage. The series resistance is given by:

$$R_{s}=\frac{kT(\gamma-n)}{qI_{min}} \quad \ldots (6)$$

where I_{min} is the current in the diode corresponding to voltage V_{min}.

Figure 2 shows plots of the Norde's function $F(V)$ versus V of the MIS diode as a function of forward applied voltage. As seen in Fig. 3, these plots give a minimum point at each temperature. As seen in Table 1, the barrier height value increases with increasing temperature. The obtained Φ_b values are in good agreement with the values obtained from the forward-bias ln$I$-V plots. As seen in Table 1, the decrease of R_s value with increasing temperature is attributed to the recombination of carriers with increasing temperature and freeze-out effects at low temperature[29].

Alternatively, to obtain the barrier height in another way, the conventional Richardson plot [ln(I_o/T^2) versus q/kT] is drawn. Equation (2) can be rewritten as:

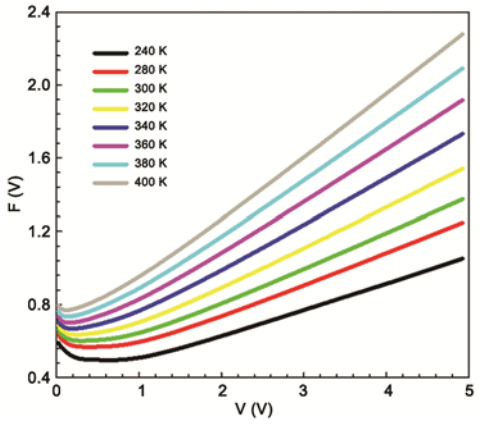

Fig. 2 — Plots of F(V) versus V of the MIS diode.

Table 1 — Electrical parameters determined from forward-bias ln$I$-V plots and Norde's function of the MIS diode.

Temperature (K)	I_0 (I-V) (A)	n (I-V)	Φ_b(I-V) (eV)	Φ_b (Norde) (eV)	R_s (Norde) (Ω)
240	4.77×10^{-7}	5.31	0.55	0.55	91.30
280	3.37×10^{-6}	4.34	0.61	0.62	64.64
300	8.04×10^{-6}	3.82	0.63	0.65	58.19
320	1.54×10^{-5}	3.24	0.66	0.69	44.62
340	2.89×10^{-5}	2.72	0.69	0.71	41.35
360	5.58×10^{-5}	2.32	0.71	0.73	38.33
380	1.06×10^{-4}	2.02	0.73	0.75	36.67
400	2.02×10^{-4}	1.75	0.75	0.79	34.79

$$\ln\left(\frac{I_0}{T^2}\right)=\ln(A\,A^*)-\frac{q\Phi_b}{kT} \quad \ldots (7)$$

Richardson plot of the MIS diode is given in Fig. 4. As seen in Fig. 3, the plot gives a straight line in the temperature range of 240-400 K. The activation energy (E_a) obtained from slope of this straight line was found to be 0.255 eV. The Richardson constant (A^*) obtained from intercept at the ordinate of this plot was found to be 5.44×10^{-5} A.cm^{-2}.K^{-2}. This value is much lower than the known theoretically value of 112 A.cm^{-2}.K^{-2} for *n* type Si. This difference is attributed to the spatially inhomogeneous barrier heights and potential fluctuations at the contact interface[6,21,22,30-33].

The abnormal deviation from ideal TE can be explained by assuming a Gaussian distribution (GD) of barrier height (BH). The barrier height with a mean barrier height ($\bar{\Phi}_b$) and standard deviation (σ_s) is given by[30-33]:

$$\Phi_b=\bar{\Phi}_b-\frac{q\sigma_S^2}{2kT} \quad \ldots (8)$$

To obtain an evidence of a GD of the BHs, Φ_b versus $q/2kT$ plot was drawn and given in Fig. 4. As seen in Fig. 4, this plot gives a straight line. The mean barrier height and standard deviation are determined from the *y*-axis intercept and slope of the Φ_b versus $q/2kT$ plot. The value of $\bar{\Phi}_b$ and σ_s was found to be 1.040 eV and 0.144 eV, respectively. The standard deviation is a measure of the homogeneity of the Schottky barrier. The obtained lower σ_s value indicates the presence of barrier inhomogeneities at the interface.

The conventional Richardson plot based on the thermionic emission deviates from linearity at low temperatures due to the barrier inhomogeneity. Therefore, the modified Richardson plot [$\ln(I_o/T^2)$-$q^2\sigma_0^2/2k^2T^2$ versus $1000/T$] is expressed by the following relation:

$$\ln\left(\frac{I_0}{T^2}\right)-\left(\frac{q^2\sigma_0^2}{2k^2T^2}\right)=\ln(A\,A^*)-\frac{q\bar{\Phi}_b}{kT} \quad \ldots (9)$$

The modified Richardson plot should be a straight line with the slope and the intercept at the ordinate directly yielding the zero-bias mean barrier height ($\bar{\Phi}_b$) and Richardson constant (A^*). Figure 5 shows modified Richardson plot of the MIS diode. As seen in Fig. 5, this plot gives a good linearity over the whole temperature range. The value of $\bar{\Phi}_b$ and A^* is found to be 1.039 eV and 113.82 A.cm^{-2}.K^{-2}, respectively. The obtained Richardson constant value is close to the theoretical value of 112 A.cm^{-2}.K^{-2} for *n*-Si.

The interface state density (N_{ss}) of the MIS diode can be obtained from the following equation[1,34]:

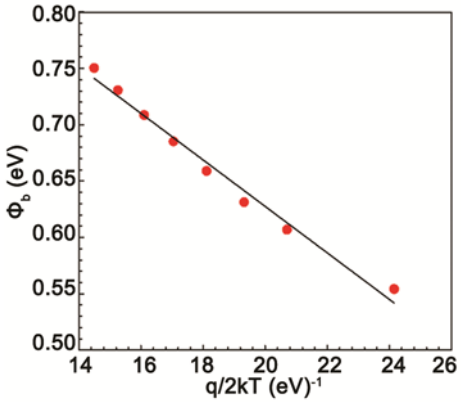

Fig. 4 — Barrier height (Φ_b) versus $q/2kT$ plot of the MIS diode.

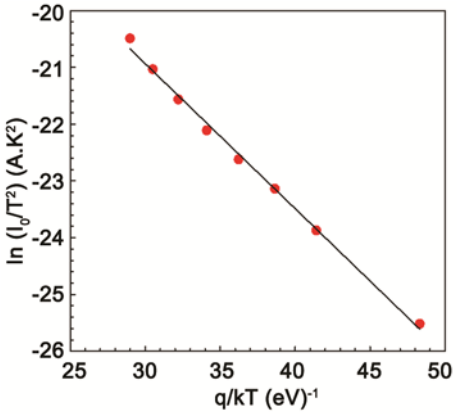

Fig. 3 — Richardson plot of the MIS diode.

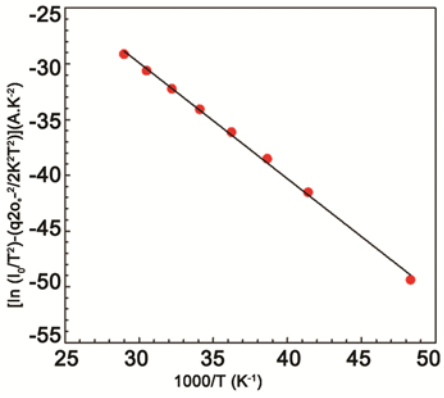

Fig. 5 — Modified Richardson plot of the MIS diode.

$$n(V) = 1 + \frac{\delta}{\varepsilon_i}\left[\frac{\varepsilon_s}{W_d} + qN_{ss}(V)\right] \quad \ldots (10)$$

where δ is the thickness of interfacial insulator layer, W_d is the space charge region width, ε_i and ε_s are the dielectric constant of the interfacial layer and the semiconductor, respectively. In *n*-type semiconductors, the energy of the interface states (E_{ss}) with respect to the bottom of conduction band is given by:

$$E_c - E_{ss} = q(\Phi_e - V) \quad \ldots (11)$$

where Φ_e is the effective barrier height related to the applied voltage and the ideality factor. The Φ_e is given by the following equation:

$$\Phi_e = \Phi_{B0} + \beta(V) = \Phi_{B0} + \left[1 - \frac{1}{n}\right](V) \quad \ldots (12)$$

where β is the voltage coefficient of Φ_e.

Figure 6 shows the plots of N_{ss} as a function of (E_c-E_{ss}) at various temperatures for the MIS diode. As seen in Fig. 6, the N_{ss} value decreases with increasing E_c-E_{ss} value for all temperatures. Also, the N_{ss} is changed with temperature. This suggests that the temperature rearrange the interfacial states of the diode. In addition, it is observed that the N_{ss} has exponential growth from the mid gap of Si toward to the bottom of the conduction band[33,34].

3.2 Capacitance-voltage characteristics

Figure 7 shows the plots of capacitance-voltage (*C*-*V*) at various frequencies and room temperature. As seen in Fig. 7, the capacitance changes with applied voltage and frequency. The capacitance value decreases with increasing frequency in forward bias, but it remains almost constant in reverse bias. The frequency dependence of capacitance may be explained by the presence of interface states in the interface of the MIS diode. In addition, the capacitance depends on the ability of the charge carriers to follow the applied alternating current signal. As the frequency is increased, the capacitance is decreased to the same limit, as the charges on the defects no longer have time to rearrange in response to the applied voltage[2,35-41]. Therefore, the capacitance has high value at low frequencies while it has low value at high frequencies. Moreover, the *C*-*V* curves give a peak. The presence of this peak may be due to the series resistance, carriers trapped at band-tail states and change in interface states.

In MIS structures, the depletion layer capacitance is given as follows[2,42-47]:

$$C^{-2} = \frac{2(V_0 + V)}{\varepsilon_S \varepsilon_0 q A^2 N_D} \text{ or } \frac{d(C^{-2})}{dV} = \frac{2}{\varepsilon_S \varepsilon_0 q A^2 N_D} \quad \ldots (13)$$

where V_0 is the built-in potential which is determined from the extrapolation of the linear C^{-2}-V plot to the V axis, ε_s is the dielectric constant of the semiconductor, N_D is the donor concentration. The diffusion potential (V_D) at zero bias is given by:

$$V_D = V_0 + \frac{kT}{q} \quad \ldots (14)$$

The barrier height (Φ_b) is calculated by the following equation:

$$\Phi_b(C-V) = V_D + E_F - \Delta\Phi_b = V_D + \left(\frac{kT}{q}\right)\ln\left(\frac{N_C}{N_D}\right) - \Delta\Phi_b \quad \ldots (15)$$

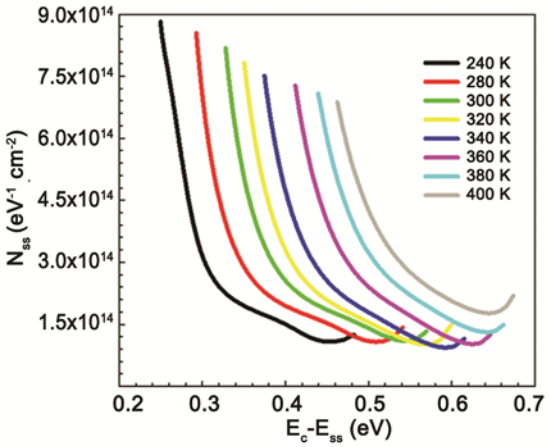

Fig. 6 — Plots of N_{ss} versus E_c-E_{ss} of the MIS diode at various temperatures.

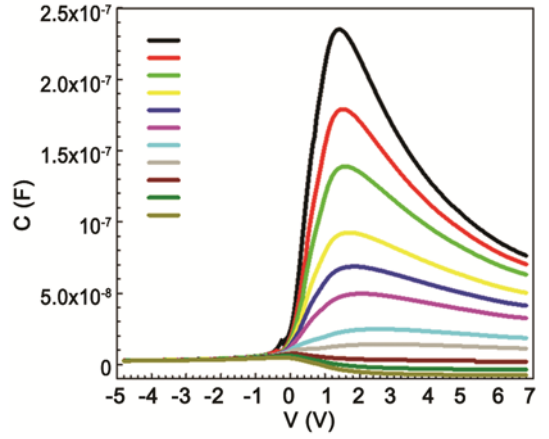

Fig. 7 — Plots of capacitance as a function of voltage at various frequencies.

Table 2 — Electrical parameters obtained from C^{-2}-V characteristics of the MIS diode.

f (Hz)	V_o(V)	V_D(eV)	N_D ($\times 10^{17}$ cm^{-3})	E_F (eV)	$\Delta\Phi_b$(eV)	Φ_b (eV)	W_D ($\times 10^{-6}$ cm)
10	0.188	0.214	4.606	0.106	0.046	0.274	2.471
20	0.188	0.214	4.551	0.107	0.046	0.274	2.487
30	0.184	0.210	4.514	0.107	0.045	0.271	2.472
50	0.184	0.210	4.475	0.107	0.045	0.271	2.483
70	0.383	0.409	4.341	0.108	0.053	0.463	3.520
100	0.386	0.412	4.328	0.108	0.053	0.466	3.539
200	0.411	0.437	4.347	0.108	0.054	0.491	3.639
300	0.442	0.468	4.352	0.108	0.055	0.520	3.761
500	0.545	0.571	4.412	0.107	0.058	0.620	4.127
700	0.704	0.730	4.503	0.107	0.062	0.775	4.619
1000	0.925	0.951	4.757	0.105	0.067	0.989	5.132

where E_F is the energy difference between the bulk Fermi level and conduction band edge, and $\Delta\Phi_B$ is the image force barrier lowering. The depletion layer width (W_D) is given by the following equation:

$$W_D = \sqrt{\frac{2\varepsilon_s\varepsilon_0 V_D}{qN_D}} \quad \ldots (16)$$

Figure 8 shows the C^{-2}-V characteristics of the MIS diode at various frequencies. As seen in Fig. 8, the C^{-2}-V curves are linearly changed with reverse voltage. The electrical parameters determined from the C^{-2}-V characteristics are given in Table 2. As seen in Table 2, the barrier height values are varied from 0.274 to 0.989 eV. It is found that the barrier height obtained from C-V measurements at 1 MHz is bigger than those obtained from the I-V measurements at 300 K. The barrier height values obtained from two methods are not always the same. The C-V method averages over the whole area and measures Schottky barrier diode. The barrier height obtained from the I-V method includes any barrier lowering effect due to the interfacial insulator layer or the interface states and yields an effective barrier height[31,48,49].

4 Conclusions

The electrical characteristics of Au/TiO_2/n-Si (MIS) diode prepared by magnetron sputtering technique were studied in detail. The MIS diode demonstrated a good rectifying behaviour. The main electrical parameters of the MIS diode were calculated from the I-V and C-V measurements. The temperature dependence of the ideality factor and the barrier height has been attributed to the barrier height inhomogeneities. The series resistance and interface state density values have obtained from Norde and I-V method, respectively. The barrier heights values obtained from the I-V and C-V method have been compared and found to be different. This difference has been attributed to the barrier inhomogeneity, the interface states and interfacial insulator layer. As result, the temperature-dependent electrical characteristics can be explained on the basis of thermionic emission mechanism with Gaussian distribution of the Schottky barrier heights.

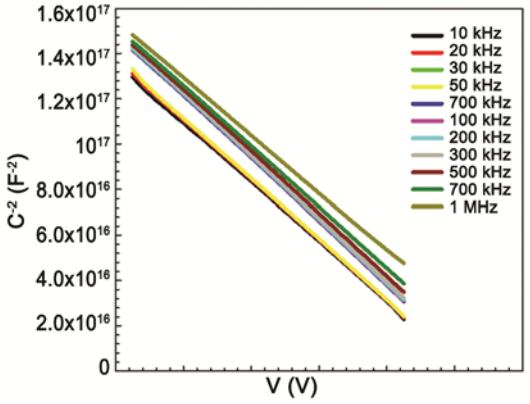

Fig. 8 — C^{-2}-V characteristics of the MIS diode at various frequencies.

Acknowledgement

This work is supported by Gazi University Scientific Research Project (BAP) with the research Project Number 05/2016-15.

References

1 Rhoderick E H & Williams R H, *Metal-semiconductor contacts*, (Clarendon Press: Oxford), 1988.
2 Sze S M, *Physics of semiconductor devices*, (John Wiley & Sons: New York), 1981.
3 Sharma B L, *Metal-semiconductor schottky barrier junctionsand their applications*, (Plenum Press: New York), 1984.
4 Tataroğlu A & Altındal S, *J Alloys Compd*, 479 (2009) 893.
5 Tung R T, *Phys Rev B*, 64 (2001) 205310.
6 Hudait M K & Krupanidhi S B, *Solid-StateElectron*, 44 (2000) 1089.

7 Elgazzar E, Tataroglu A, Al-Ghamdi A A, Al-Turki Y, Farooq W A, El-Tantawy F & Yakuphanoglu F, *Appl Phys A*, 122 (2016) 122.
8 Karatas S, Altındal S, Turut A & Cakar M, *Physica B*, 392 (2007) 43.
9 Umapathi A & Reddy V R, *Microelectron Eng*, 114 (2014) 31.
10 Mamor M, Bouziane K, Tirbiyine A & Alhamrashdi H, *Superlattices Microstruct*, 72 (2014) 344.
11 Yakuphanoglu F, Okutan M & Korkmaz K, *J Alloys Compd*, 450 (2008) 39.
12 Tian J, Gao H, Deng H, Sun L, Kong H, Yang P & Chu J, *J Alloys Compd*, 581 (2013) 318.
13 Huang H, Jiang L, Zhang W K, Gan Y P, Tao X Y & Chen H F, *Sol Energy Mater Sol Cells*, 94 (2010) 355.
14 Kınacı B & Özçelik S, *J Electron Mater*, 42 (2013) 1108.
15 Addepalli S & Suda U, *Bull Mater Sci*, 39 (2016) 789.
16 Bengi A, Aydemir U, Altındal S, Ozen Y & Ozcelik S, *J Alloys Compd*, 505 (2010) 628.
17 Mergel D, Buschendorf D, Eggert S, Grammes R & Samset B, *Thin Solid Films*, 371 (2000) 218.
18 Bernardi M I B, Lee E J H, Lisboa-Filho P N, Leite E R, Longo E & Varela J A, *Mater Res*, 4 (2001) 223.
19 Pessoa R S, Pereira F P, Testoni G E, Chiappim W, Maciel H S & Santos L V, *J Integr Circuits Syst*, 10 (2015) 38.
20 Long H, Chen A, Yang G, Li Y & Lu P, *Thin Solid Films*, 517 (2009) 5601.
21 Moraki K, Bengi S, Zeyrek S, Bülbül M M & Altindal S, *J Mater Sci: Mater Electron*, 28 (2017) 3987.
22 Tataroğlu A & Pür F Z, *Phys Scr*, 88 (2013) 015801.
23 Ocaya R O, Al-GhamdiAhmed, El -Tantawy F, Farooq W A & Yakuphanoglu F, *J Alloys Compd*, 674 (2016) 277.
24 Chen J, Lv J &Wang Q, *Thin Solid Films*, 616 (2016) 145.
25 Ouennoughi Z, Toumi S & Weiss R, *Physica B*, 456 (2015) 176.
26 Kumar R & Chand S, *Solid State Sci*, 58 (2016) 115.
27 Norde H, *J Appl Phys*, 50 (1979) 5052.
28 Sato K & Yasumura Y, *J Appl Phys*, 58 (1985) 3655.
29 Chand S & Kumar J, *J Appl Phys*, 63 (1996) 171.
30 Tung R T, *Mater Sci Eng R*, 35 (2001) 1.
31 Werner J H & Guttler H H, *J Appl Phys*, 69 (1991) 1522.
32 *Chand S & Kumar J, Semicond Sci Technol*, *10* (1995) *1680.*
33 Khurelbaatar Z, Shim K H, Cho J, Hong H, Reddy V R & Choi C J, *Mater Trans*, 56 (2015) 10.
34 Card H C & Rhoderick E H, *J Phys D*, 4 (1971) 1589.
35 Nicollian E H & Brews J R, *MOS physics and technology*, (Wiley: New York), 1982.
36 Cova P & Singh A, *Solid-State Electron*, 33 (1990) 11.
37 Tataroglu A, Al-Ghamdi A A, El-Tantawy F, Farooq W A & Yakuphanoglu F, *Appl Phys A*, 122 (2016) 220.
38 Kim H, Kim H & Kim D W, *Vacuum*, 101 (2014) 92.
39 Tataroglu B, Altındal S & Tataroglu A, *Microelectron Eng*, 83 (2006) 2021.
40 Kahraman A, Yilmaz E, Kaya S & Aktag A, *J Mater Sci: Mater Electron*, 26 (2015) 8277.
41 Nath M & Roy A, *Physica B*, 482 (2016) 43.
42 Tataroğlu A & Altindal S, *Vacuum*, 82 (2008) 1203.
43 Aydın M E & Yakuphanoğlu F, *Microelectron Reliab*, 52 (2012) 1350.
44 Dutta D P & Sharma G, *Mater Sci Eng B*, 176 (2011) 177.
45 Orak I, Kocyigit A & Turut A, *J Alloys Compd*, 691 (2017) 873.
46 Saghrouni H, Hannachi R, Jomni S & Beji L, *Physica B*, 422 (2013) 64.
47 Padma R, Sreenu K & Rajagopal R V, *J Alloys Compd*, 695 (2017) 2587.
48 Janardhanam V, Lee H K, Shim K H, Hong H B, Lee S H, Ahn K S & Choi C J, *J Alloys Compd*, 504 (2010) 146.
49 Coskun C, Aydogan S & Efeoglu H, *Semicond Sci Technol*, 19 (2004) 242.